Low Speed Numerical Aerodynamic Analysis of New Designed 3D Transport Aircraft

Hacı Sogukpinar

Department of Electric and Energy, Vocational School,
University of Adiyaman, Adiyaman 02040, Turkey
(hsogukpinar@adiyaman.edu.tr)

‡Corresponding Author; Hacı Sogukpinar, Department of Electric and Energy, Vocational School, University of Adiyaman, Adiyaman 02040, Turkey, Tel: +90 (416) 223 38 00,

Fax: + 90 416 223 21 29, hsogukpinar@adiyaman.edu.tr

Received: 27.02.2018 Accepted: 13.01.2019

Abstract - In this study, a new airfoil was designed by using aerodynamic features of the NACA (National Advisory Committee for Aeronautics) 0012 airfoil and numerical calculation was conducted by using Spalart–Allmaras Turbulence Model. Lift and drag coefficients were calculated and compared with experimental result to correlate numerical calculation accuracy of CFD (Computational Fluid Dynamics) model. Then, according to the new airfoil data, a 3D aircraft fuselage, wings and tail section were modeled by using modified NACA 0012 airfoil. Finally, 3D model aircraft were simulated for cruise flight, climb and descending at the angle of attack +10° and -10° respectively. The simulation results were interpreted in terms of fluid dynamics. Study indicates that during the ascending and descending of the aircraft, very large vortices were formed by the low pressure effect occurring at the rear upper or lower part of the fuselage. Vortices originating from the rear body were caused with the wing tip vortices but the vortex due to the back of the fuselage was found to be very large compared to the wingtip. Furthermore, for each simulation, formation of the wingtip vortices were investigated and presented. Study shows that during ascending the vortex formation was formed in roll up but it was roll down in the phase of descending.

Key words: 3D simulation, Aircraft, vortex, airfoil, Aerodynamic Analysis, lift, drag

1. Introduction

After the first flight of the Wright brothers, new sectors has emerged and research in the whole aviation continued rapidly. As a result of great efforts, dream of the larger airplane and longer distance flights has become real. The high cost of fuel and global warming effects made the need for more efficient airplanes in terms of aerodynamics, and the work has progressed in this direction. Especially at airports, vortices formed during landing and takeoff which affect other flight negatively. For the last 30 years, winglets have been developed and used to reduce wingtip vortex. Aerodynamic flow as a whole for an aircraft has not been investigated but usually only the flow over the wing, the fuselage, the tail and winglet were investigated. But within the framework of an agreement between NASA (National Aeronautics and Space Administration) and Boeing, Boeing 747 passengers' aircraft were analyzed numerically as a whole and presented [1]. The document provides aerodynamic features of lift, drag, pitching moment, rolling and yawing moment, and side force coefficients and also contains information about characteristics of the high lift and propulsion system and landing gear. However, the presented data handles in the form of numeric data and graphs but there is no 2D or 3D direct stream graphics. Flow over generic military airplane was simulated as a whole by using SST turbulence model and compared with experiment [2]. Velocity distribution and eddy viscosity on the surface of the aircraft were given visually and comparatively with the experiment and there was a good agreement between numerical calculation and observation. The main purpose of that work was only to summarize the role of the concepts behind the SST model in current and future CFD simulations of engineering flows. The Boeing 747-200 jumbo jet was numerically investigated and the pressure distribution over the entire surface of the aircraft presented [3]. But the velocity distribution of

the fluid sweeping the surface of the plane was not calculated or given. Therefore, places where swirls are not seen. Another investigation explains the application of optimization techniques for based on control theory for complex aircraft configurations [4] and numerical calculation was conducted for business jet by using Euler equations. This method used Euler equations to reconstruct all configurations of the aircraft by using new multi-block implementation. According to the calculation result, pressure distribution on the entire surface of the plane was presented. With the development of current computer technology CFD's practice revolutionized the aerodynamic design process and it has joined the wind tunnel and flight test as the main means of trade. Boeing Commercial Airplanes use CFD technology, developed by its academia and NASA, and has been used in new plane development. More than 20,000 CFD cases were completed to design a new aircraft in Boeing Company [5]. In other studies, 2D and 3D wing sections were studied extensively [6-12], but it is quite rare to investigate the 3D shape of a plane for aerodynamic analysis. Especially, flow analysis was rarely performed by sending fluid from different angles to the aircraft surface.

In this study, a new airfoil with high lift coefficient at angle of attack zero degree was modeled by using aerodynamic characteristics of NACA 0012 airfoil. The NACA 0012-X airfoil was compared both experimental and theoretical NACA 0012 data to check the simulation correctness of the Computational Fluid Dynamics (CFD) approximation. The airplane fuselage and wings were created using the NACA 0012-X airfoil and numerical calculation conducted by using the Spa-Almrs turbulence model. The streamline velocity distribution on the wing and fuselage were presented and compared according to the simulation result.

2. Spalart–Allmaras Turbulence Model

The Spalart-Allmaras model is a one-equation model that solves a modeled transport equation for the kinematic eddy turbulent viscosity. The model solves only one transport equation for the quantity $\tilde{v}$, it is equivalent to the eddy viscosity away from the walls [13]. This model was designed specifically for aerospace applications that include wall-bounded flows and has been shown to provide good results for boundary layers exposed to negative pressure gradients. This module includes the standard version of the Spalart-Allmaras model without trip term [14, 15]. One model equation for undamped turbulent kinematics is given by equation (1):

$$\frac{\partial \tilde{v}}{\partial t} + \mathbf{u}.\nabla\tilde{v} = c_{b1}\widetilde{S\nu} - c_{w1}f_w\left(\frac{\tilde{v}}{l_w}\right)^2 + \frac{1}{\sigma}\nabla.\left((v+\tilde{v})\nabla\tilde{v}\right) + \frac{c_{b2}}{\sigma}\nabla\tilde{v}.\nabla\tilde{v} \quad (1)$$

Reynold stresses were evaluated by using Boussinesq eddy viscosity assumption [16] and are expressed by (2):

$$c_{w1} = \frac{c_{b1}}{\kappa_v^2} + \frac{1+c_{b2}}{\sigma}, \chi = \frac{\tilde{v}}{v}, f_{w1} = \frac{\chi^3}{\chi^3 + {c_{v1}}^3} \quad (2)$$

The turbulent viscosity was calculated by (3):

$$\mu_T = \rho\tilde{v}f_{v1} \quad (3)$$

To achieve faster decaying behavior of destruction in the outer boundary layer, a function $f_w$was used [17].Additional definitions were given in the following equations (4-6) where g acts as a limiter that prevents great values of f_w. Both r and f_w are equal to 1 in the log-layer and decrease in the outer region.

$$f_{w2} = 1 - \frac{\chi}{1+\chi f_{v1}}, f_w = g\left(\frac{1+c_{w3}^6}{g^6+c_{w3}^6}\right)^{1/6}, g = r + c_{w2}(r^6 - r) \quad (4)$$

$$r = min\left(\frac{\tilde{v}}{\tilde{S}\kappa^2{}_v l^2{}_w}, 10\right), \tilde{S} = max\left(\Omega + C_{Rot}\min(0, S-\Omega) + \frac{\tilde{v}}{\kappa^2{}_v l^2{}_w}f_{v2}, 0.3\Omega\right) \quad (5)$$

$$S = \sqrt{2S_{ij}S_{ij}} \quad \Omega = \sqrt{2\Omega_{ij}\Omega_{ij}} \quad (6)$$

Where, $f_{w1}$is damping fuction, κ is von Kármán constant, $\tilde{S}$ is modified vorticity, S is magnitude of vorticity, l_w is distance to the closest wall, $\tilde{v}$, is kinematic viscosity, $S_{ij}$and Ω_{ij} are mean strain rate and mean rotation rate tensors respectively and represented by:

$$S_{ij} = 0.5(\nabla u + \nabla u^T)\Omega_{ij} = 0.5(\nabla u - \nabla u^T) \quad (7)$$

The default value of model constants are:

$c_{b1} = 0.1355, c_{b2} = 0.622, c_{v2} = 7.1\sigma = {}^2/_3$

$c_{w2} = 0.3,\ c_{w3} = 2, \kappa_v = 0.41, C_{Rot} = 2.0$

3. CFD Modeling method

NACA 0012 is one of the commonly used airfoil due to its aerodynamic properties. Hundreds of experimental and theoretical investigations have been carried out for this wing section. Wind tunnel experiment of NACA 0012 was conducted in the Langley Low-Turbulence Pressure Tunnel [18] to investigate the low-speed aerodynamic characteristics of the NACA 0012 airfoil, which offers good opportunity to examine CFD simulation technicque. For the numerical calculation Commercial software COMSOL 5.3 was used. To eliminate the effect of the domain size on the numerical simulation, computational domain and boundary conditions extended at least 100c away from airfoil. Computational domain is as shown in Fig. 1. Inlet port was set to velocity inlet and output port was set to output. Low number mesh distribution may produce computation with large error but high number mesh increase computational time. Therefore mesh number in acertain range were used which is compatible with experiment. C type mesh with 86,800 mesh element were created and applied to distribute flow field in the domain and free stream contiditon. High concentrated mesh distribution was applied closed to wall. Mesh distribution around new designed airfoil NACA 0012-X is presented in Fig.2.

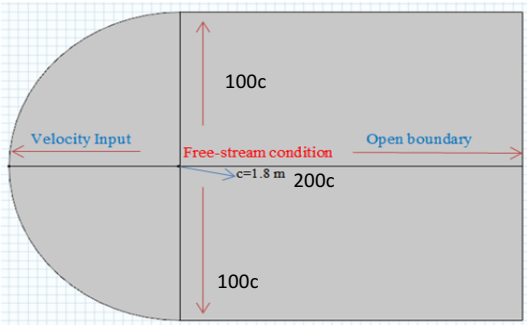

Fig. 1: Computational domain and boundary condition.

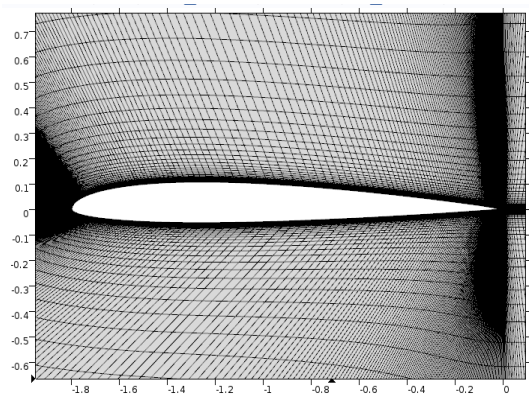
Fig. 2. Mesh distribution around airfoil NACA 0012-X

The model fuselage was designed according to the NACA 0012-X profile, with a chord length of 1 m. Aircraft wing was designed from NACA 0012-X airfoil with 1.1 m wing span. Wing incidence was set to 3°. The leading edge sweep was depicted as 8.5°. Zero twist and dihedral angle were applied to the model. Basic tail configuration with NACA 0012 airfoil was adopted. For the 3D calculation, separate mesh distribution for the model aircraft and the external environment were applied and free tetrahedral mesh type with extra fine mesh was adopted for both side. 3D body of model with mesh distribution is presenten in Fig. 3.

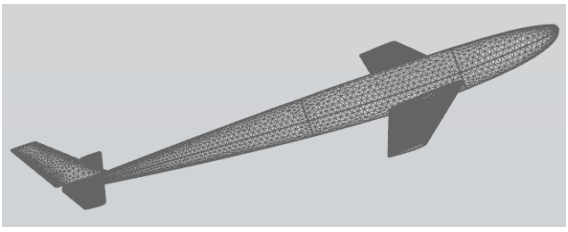
Fig. 3. Mesh distribution around aircraft modeled from NACA 0012-X

4. Results and discussions

Numerical calculation was conducted for NACA 0012 airfoil and lift and drag coefficients were calculated with Spalart–Allmaras turbulence model with the angle of attack from -4° to +18° and presented in Fig. 4, and obtained data were compared with experimental observation [18]. It is observed that theoretical results are in a good agreement with the experimental results. An airfoil with an aerodynamic characteristic close to NACA 0012 but with a high lift coefficient was designed and named as NACA 0012-X. The newly designed airfoil was simulated by using the Spalart-Allmaras Turbulence Model and compared with theoretical and experimental data of NACA 0012 as presented in Fig.4. According to the simulation results, high lift coefficient were obtained in all angle of attack and lift coefficients were calculated at the angle of attack at 0° and 3° as 0.16 and 0.49 respectively.

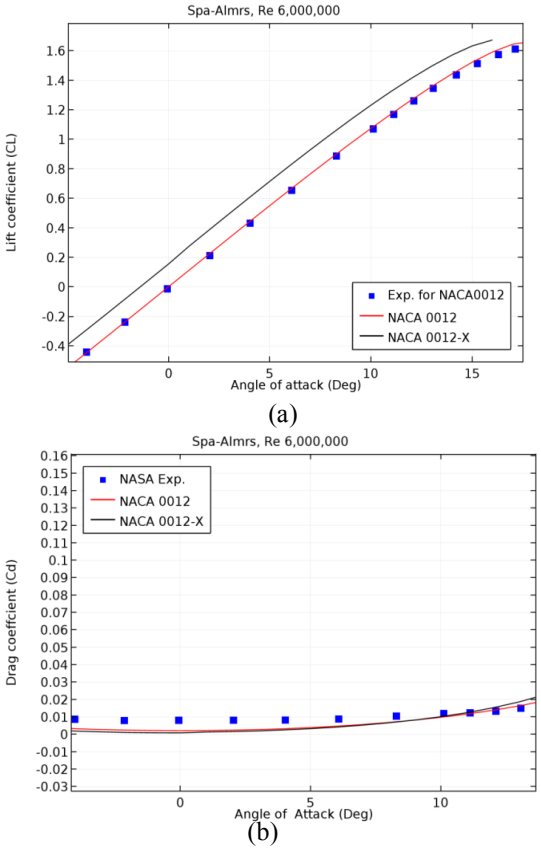

Fig. 4. Comparison of Lift and Drag coefficient versus angle of attack.

Drag coefficient for newly designed airfoil was calculated lower than both experiment and theoretical data of NACA 0012 airfoil at the angle of attack until 11°. Lift to drag ratio for NACA 0012-X airfoil were calculated and presented comparatively with NACA 0012 airfoil in Fig. 5. Maximum lift to drag ratio was calculated at the angle of attack around 3° therefore streamline velocity is also presented in Fig.5(b).

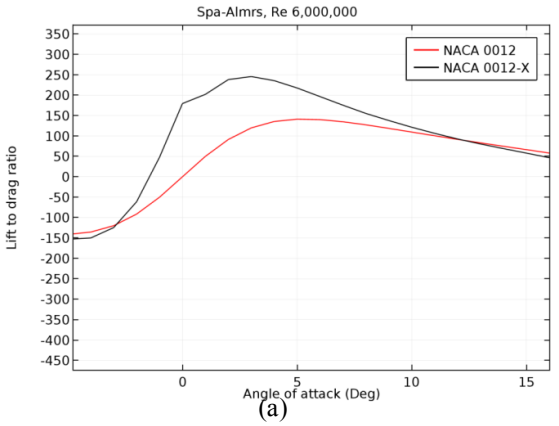

(a)

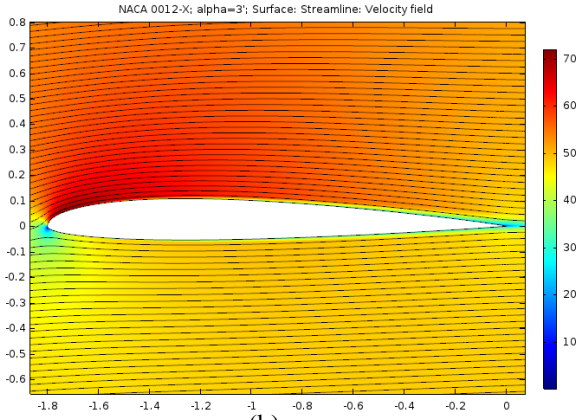

(b)

Fig. 5. Lift to drag ratio (a) and streamline velocity field (b) of NACA0012-X

The stream line velocity field of the NACA 0012-X airfoil is given in Fig.6 at the angle of attack 12° and 14° and almost laminar flows are calculated in both Fig. 6(a) and Fig. 6(b) but the flows separation starts on the upper rear side of airfoil. The low pressure region (reddish) in both images shifted to the front side of the airfoil, which increase the drag as expected to do. Since the low pressure is on leading edge side of airfoil so low pressure pulls wing to that side therefore this automatically increases drag coefficient. The lift coefficients were calculated as 1.41 and 1.57, and the drag coefficients were 0.015 and 0.022, at the angle of attack 3°for the NACA 0012 and NACA 0012-X.

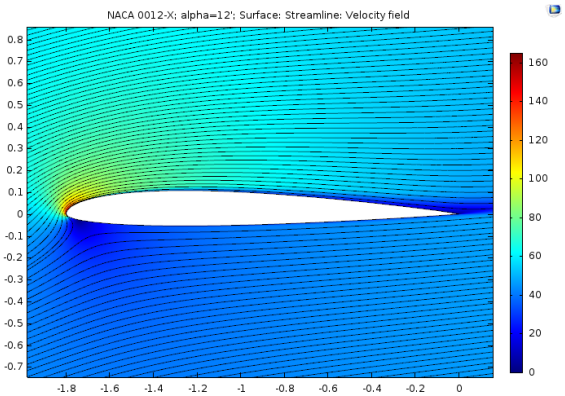

(a)

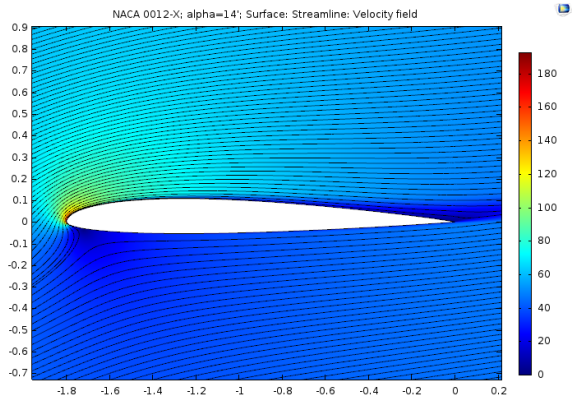

(b)

Fig. 6. Streamline velocity fields for NACA 0012-X

Model aircraft fuselage and wings were designed using NACA 0012-X airfoil and tail section was made from NACA 0012. Numerical calculations were performed for model airplane using Spalart-Allmaras Turbulence Model at the angle of attack zero but the maximum lift to drag ratio was achieved at 3° therefore wing incidence was set to 3 °. 3D streamline velocity field of model with top and bottom view is as shown in Fig. 7 and side view is shown in Fig. 8. The graph was plotted by sending fluids over the top and bottom of the wing surface a sequence of layer on the x-y plane. As shown in Fig. 7 and Fig. 8, air flows faster at the top of the plane (reddish color) and slower at the bottom (light color) and laminar flow formed on both sides and fluid continues to sweep the surface of the aircraft front to back properly. Along the fuselage surface, fluid is seen in light color because no slip boundary condition was applied.

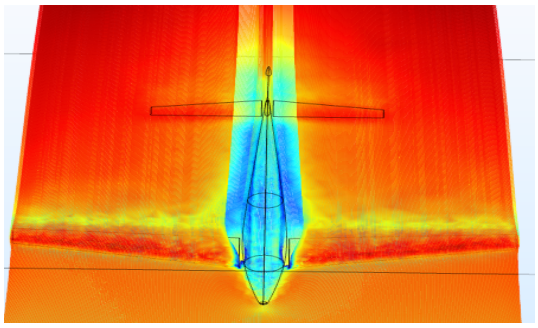

(a)

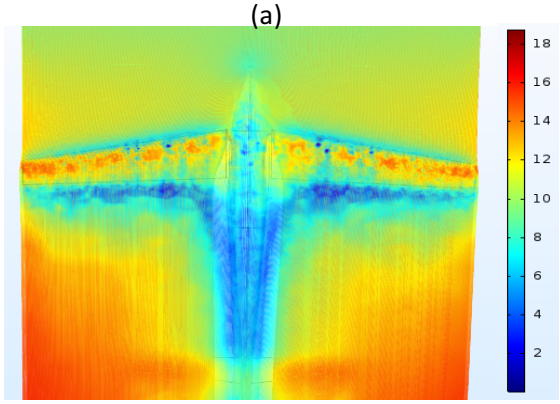

(b)

Fig. 7. 3D streamline velocity field of model with top (a) and bottom (b) view.

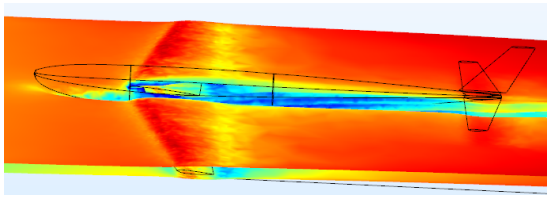

Fig. 8. 3D streamline velocity field of model with side view.

The fluid was sent as a single layer on x-z plane along the model aircraft and is shown in Fig. 9. It should be emphasized that the fluid only moves over the fuselage and there is no flow on the wing and tail. As we compare the color distribution of the fluid, it is observed that the fluid moves at equal speeds on the top and bottom of the fuselage but fluid moves more slowly behind the plane and along the fuselage surface because of the shadow effect and the no-slip condition respectively.

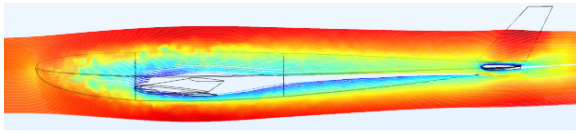

Fig. 9. 3D streamline velocity field over fuselage with side view.

The wingtip vortex was calculated by sending fluid on the x-z plane along the wing surface and is given in Fig. 10. The wingtip vortex formation is enlarged and shown in the same Fig. 10. Due to the pressure difference at the top and bottom of the wing, air flow rolls up into large vortices near the wingtip as seen in Fig. 10. There is no angle of incidence of the plane, but only the wings have three degrees of incidence. Therefore the wingtip vortex is seen to be less in the cruise flight.

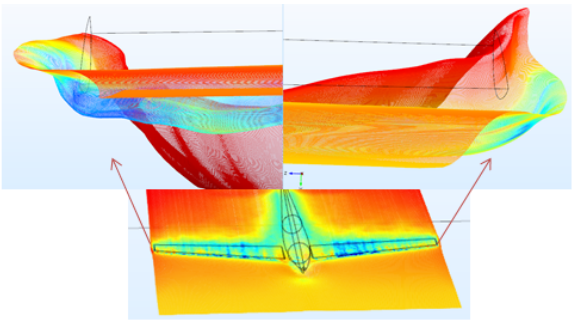

Fig. 10. Wingtip vortex at 3° wing incidence at cruise flight.

Numerical calculation was carried out by giving a 10° angle of attack to the model aircraft and top rear view and top front view are shown in Fig.11 and Fig.12 respectively.

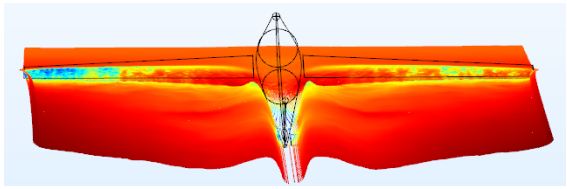

Fig. 11. Top rear view of climbing aircraft at the angle of 10°.

As it is shown in Fig. 11, the formation of the wingtip vortex is clearly visible, but a much larger formation of vortex occurs at the rear of the body. When the plane ascending, it forms a low pressure region at the upper back of the fuselage. And this region leads to the formation of wave peaks from bottom to top. These apices move outward from the body and turn into gigantic vortex waves combining with wingtip vortex at the back of the plane. When the image from the upper front of a flight ascending at the angle of attack 10° is given in Fig. 12, it appears that the vortex formed at the rear of the body is larger than the wingtip vortex.

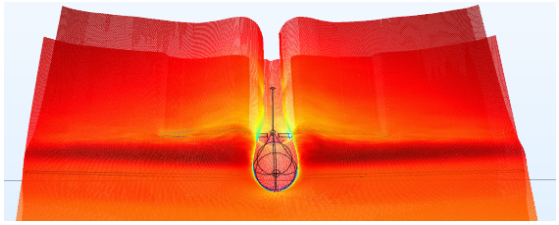

Fig. 12. Top front view of climbing aircraft at the angle of 10°.

The lateral-top and bottom-front views of the plane rising at an angle of 10 ° are given in Fig. 13 and Fig. 14, respectively. When Fig. 13 and Fig.14 are examined, fluid rises to the low pressure region of the back upper part of the body and forms wave peaks. The vortex formed at the upper back of the body is very large compared to the wingtip vortex as shown in Fig.13.

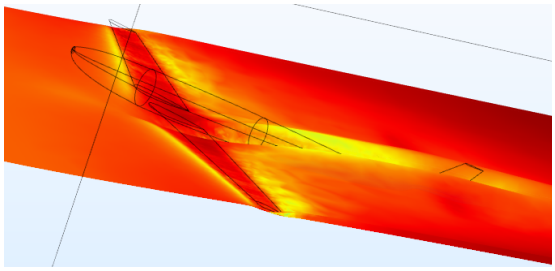

Fig. 13. Lateral top view of climbing aircraft at the angle of 10°.

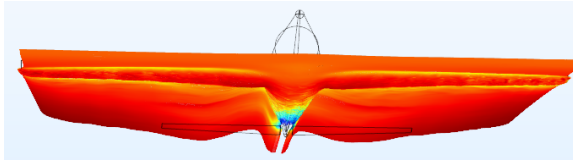

Fig. 14. Sub front view of climbing aircraft at the angle of 10°.

A close-up side view of the fluid passing through the wing surface is shown in Fig. 15. It is seen in Fig. 15 that the fluid passing over the top of the wing continues to travel smoothly, but the fluid passing along the bottom surface curves upwards to form the wingtip vortex.

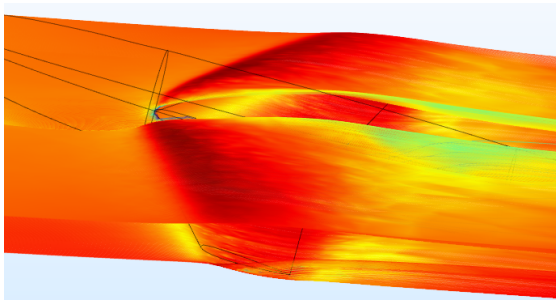

Fig. 15. A close-up side view of the fluid passing through the wing surface.

Wingtip vortex formation (Fig. 16) of the model plane ascending at the angle of attack 10° (the total wing incidence is 13°) is enlarged and for both side is given in Fig. 16. A circular pattern of rotating air is clearly visible at both side of wing.

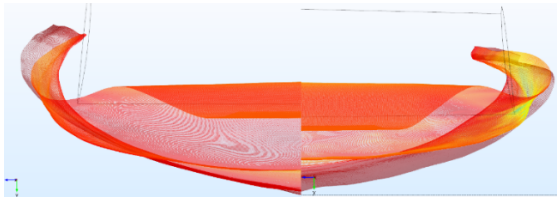

Fig. 16. Wingtip vortex formation of ascending aircraft at the angle of attack 10°.

Descending model aircraft with the angle of attack -10° was numerically analyzed and side view, lower back view, upper-front view, and Sub-front view are presented in Fig. 17, Fig. 18, Fig. 19 and Fig. 20 respectively. When the plane is tilted downward, a low pressure region is formed at the bottom of the tail (back bottom of the fuselage) as seen from the velocity distribution of the fluid (light color), and the shedding effect arises from the body, and ascending to the top of the tail. The fluid flows over the x-y plane, bends in the low pressure region and continues to create large air waves as seen in Fig 17-20. The resulting hill-shaped waves move outward from the wings, and merges with the wingtip vortex and turn into circular vortex flows behind the aircraft. It is seen that the height of the vortex (wave peak) rises from the wings towards the tail. Wingtip vortex formation of descending model plane at the angle of attack -10° (the total wing incidence is -13°) is enlarged and for both side is given in Fig. 21.The direction of the emerging wingtip vortex for the descending mode is opposite to that of the ascending aircraft as shown in Fig.16 and Fig.21.

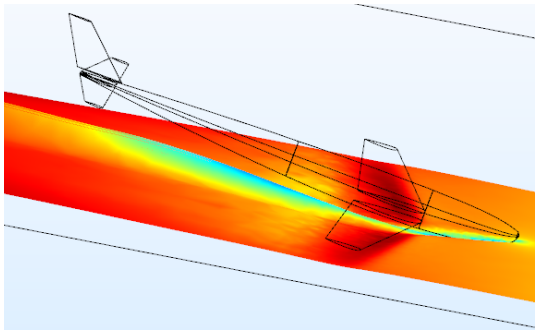

Fig. 17. Side view of descending aircraft at the angle of -10°

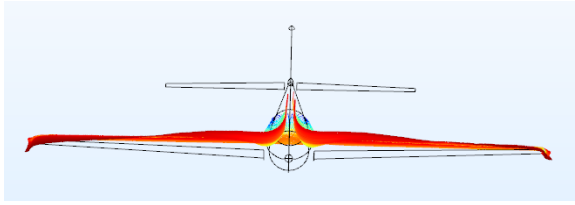

Fig. 18. Lower back side view of descending aircraft at the angle of -10°

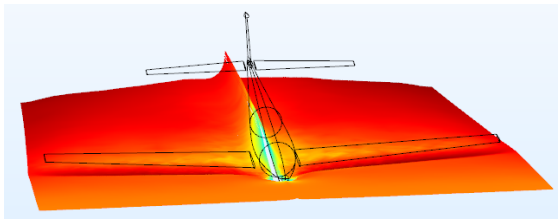

Fig. 19. Upper-front view of descending aircraft at the angle of -10°

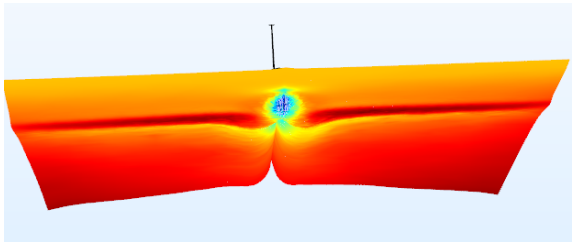

Fig. 20. Sub-front view of descending aircraft at the angle of -10°.

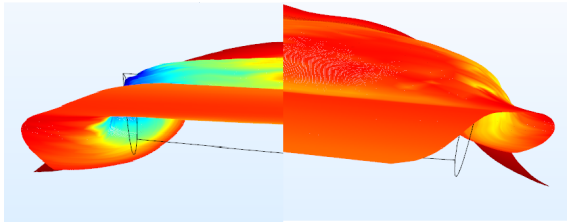

Fig. 21. Wingtip vortex formation of descending aircraft at the angle of attack -10°.

5. Conclusion

Today implementation of CFD has revolutionized the aerodynamic process. In the last 40 years, CFD has been added as a reliable tool for wind tunnel and flight test as a critical tool. Aerodynamic performance of 3D model passenger aircraft was modeled from modified NACA 0012 airfoil and were investigated by using Spalart–Allmaras Turbulence Model. First, 2D simulation data were compared with those obtained from wind tunnel experiment to correlate the simulation correctness of the Computational Fluid Dynamics (CFD) approach. Lift and drag coefficient of NACA 0012 and modified NACA 0012-X were calculated and compared with experiment and comparison shows a good agreement. Then using the newly designed airfoil, the passenger plane's wings and fuselage were created. Aerodynamic properties of the aircraft were investigated by sending air from different angles to the aircraft's wings and its fuselage. According to the result of the simulation, it is seen that during ascending or descending, large wave dips are seen on the rear side of the fuselage. According to the flow analysis, these ripples are due to the difference in pressure at the top and bottom of the tail. Wingtip vortex was also numerically analyzed and it is observed that during the ascending, wing vortex is curved upwards, and during descending it is curved down from bottom. In the flow analysis, the vortex formed at the back of the fuselage is seen to be larger and stronger compared to wingtip vortex. The vortex formed at the wingtip and at rear back of the body combine to form stronger circular vortices.

Acknowledgment

Many thanks to Middle East Technical University and Adiyaman University for technical support.

Funding

This work was supported by Adiyaman University Scientific Research Project (Project no: TEBMYOMAP/2018-0001).

References

[1] C. R. Hanke and R. N. Donald, “The Simulation Of A Jumbo Jet Transport Aircraft”,Vol.1, D6 - 30643, 1970.

[2] F.R. Menter, “Review of the shear-stress transport turbulence model experience from an industrial perspective”, International Journal of Computational Fluid Dynamics, Vol. 23:4, pp. 305-316, 2009.

[3] A. Jameson, T. J. Baker and N. P. Weatherill, “Calculation of Inviscid Transonic Flow over a Complete Aircraft”, AIAA 24th Aerospace Sciences Meeting, 86-0103. 1986.

[4] J. Reuther, A. Jameson, J. Farmer, L. Martinelli, D. Saunders, C.A. Moffett Field, “Aerodynamic shape optimization of complex aircraft configurations via an adjoint formulation”, AIAA Paper, pp. 94, 1996.

[5] T. Forrester Johnson, N. Edward Tinoco, N. Jong Yu. “Thirty years of development and application of CFD at Boeing Commercial Airplanes, Seattle”, Computers & Fluids, Vol. 34, pp. 1115–1151, 2005.

[6] H. Sogukpinar, and I. Bozkurt. "Calculation of Optimum Angle of Attack to Determine Maximum Lift to Drag Ratio of NACA 632-215 Airfoil." Journal of Multidisciplinary Engineering Science and Technology, Volume 2, pp.1103-1108, 2015.

[7] H. Sogukpinar, and I. Bozkurt, "Calculation of Aerodynamic Performance Characteristics of Airplane Wing and Comparing with the Experimental Measurement." International Journal of Engineering Technologies Volume 1.2, pp. 83-87, 2015.

[8] H. Sogukpinar, “Numerical calculation of wind tip vortex formation for different wingtip devices”, INCAS Bulletin, Volume 10(3), pp. 167-176, 2018.

[9] H. Sogukpinar, “Numerical Simulation of 4-Digit Inclined NACA 00xx Airfoils To Find Optimum Angle of Attack for Airplane Wing” Uludag University Journal of The Faculty of Engineering, Volume 22.1, pp. 169-178, 2017.

[10] H. Sogukpinar, "The effects of NACA 0012 airfoil modification on aerodynamic performance improvement and obtaining high lift coefficient and post-stall airfoil.", AIP Conference Proceedings, Vol. 1935. No. 1. AIP Publishing, 2018.

[11] H. Sogukpinar, "Estimation of supersonic fighter jet airfoil data and low speed aerodynamic analysis of airfoil section at the Mach number 0.15." AIP Conference Proceedings. Vol. 1935. No. 1. AIP Publishing, 2018.

[12] H. Sogukpinar, and Ismail Bozkurt. "Implementation of different turbulence model to find proper model to estimate aerodynamic properties of airfoils." AIP Conference Proceedings, Vol. 1935. No. 1, AIP Publishing, 2018.

[13] B. Aupoix, P.R. Spalart, “Extensions of the Spalart–Allmaras turbulence model to account for wall roughness”, International Journal of Heat and Fluid Flow, Volume 24, pp. 454–462, 2003.

[14] D.C. Wilcox, Turbulence Modeling for CFD, 2nd ed., DCW Industries, 1998.

[15] The Spalart-Allmaras Turbulence Model, NASA Langley Research Center. https://turbmodels.larc.nasa.gov

[16] S.R. Allmaras, T.J. Forrester, and P.R. Spalart. "Modifications and Clarifications for the Implementation of the Spalart-Allmaras Turbulence Model." Seventh International Conference on Computational Fluid Dynamics (ICCFD7), 2012.

[17] S. Deck, P. Duveau, P. d'Espiney, & P. Guillen, “Development and application of Spalart–Allmaras one equation turbulence model to three-dimensional supersonic complex configurations”, Aerospace Science and Technology, Volume 6(3), pp. 171-183, 2002.

[18] C.L. Ladson, “Effects of Independent Variation of Mach and Reynolds Numbers on the Low-Speed Aerodynamic Characteristics of the NACA 0012 Airfoil Section, NASA TM 4074, 1988.